Development of the numerical methods of analysis the two-particle correlations in the ALICE experiment at CERN LHC

MARCIN PATECKI

Engineer Thesis

Supervisor:
Dr hab. inż. Adam Kisiel
Faculty of Physics, Warsaw University of Technology

Warsaw, January 2012

Abstract

This thesis presents results and conclusions obtained by studying two-particle $\Delta\eta\Delta\phi$ correlation functions in proton-proton collisions at center of mass energy $\sqrt{s} = \ 7\ TeV$ recorded by the ALICE experiment. The shape of $\Delta\eta\Delta\phi$ correlation function is the result of several physical phenomena like Bose-Einstein correlation, resonances decay, photon conversion, minijets and elliptic flow. There are also some detector effects, like limited acceptance, which also contribute to the overall shape of the correlation function. My work focuses on fitting the $\Delta\eta\Delta\phi$ correlation functions in order to quantitatively describe the trends of its shape as a function of multiplicity and pair transverse momentum ($p_{T,sum}$). The main goal of the work is to extract the dominant structures in the shape of $\Delta\eta\Delta\phi$ correlation function in order to study their multiplicity and $p_{T,sum}$ dependence. This can lead to better understanding of the physical effects in pp collisions.

Fitting the $\Delta\eta\Delta\phi$ correlation function is performed with the MINUIT analysis package integrated in the ROOT environment. The procedure is based on calculating the χ^2 between the proposed fitting function and the data for given values of parameters. The task of MINUIT is to obtain the minimum value of χ^2 by finding the optimal parameters; it also provides the errors and the covariance matrix necessary in the discussion of uncertainties.

The introduced fitting formula is composed of four modified Gaussian functions, each related to certain structure of the correlation function. Modified Gaussian functions, which are more sharp and narrow, correspond better to the shapes seen in the data. It is also necessary to include a second order polynomial in the fitting formula to account for acceptance effects in $\Delta\eta$.

As a result of my studies I obtained the dependence of the parameters of the fit on the multiplicity and $\mathrm{p}_{T,sum}$. It allowed to quantitatively describe the contribution of different physical phenomena to the overall shape; however, there are situations where it is difficult to distinguish the different correlation sources.

Contents

1 Introduction **3**

1.1 Large Hadron Collider 3

1.2 ALICE Experiment 4

2 $\Delta\eta\Delta\phi$ correlation function **5**

2.1 Observables 5

2.2 Construction of $\Delta\eta\Delta\phi$ correlation function 7

2.3 Correlation sources 8

3 Experimental setup and datasets **11**

3.1 Detectors 11

3.1.1 Inner Tracking System 11

3.1.2 Time Projection Chamber 12

3.1.3 VZERO 12

3.2 Datasets 13

3.2.1 Multiplicity ranges 13

3.2.2 $p_{T,sum}$ ranges 14

3.2.3 Charge dependence 14

4 Fitting procedure **16**

4.1 Introduction 16

4.2 MIGRAD algorithm 17

4.3 Chi-square function 17

4.4 Residual histogram 17

4.5 Fitting formula 18

4.5.1 The combination of the Gaussian functions 18

4.5.2 The combination of the modified Gaussian functions 18

4.5.3 The combination of the modified Gaussian functions with the second order polynomial function 20

5 Developed software tools **22**

6 Fitting results **26**

6.1 Multiplicity dependence of the fit parameters 26

6.2 Transverse momentum dependence of the fit parameters 27

7 Analysis of uncertainties **30**

7.1 Polarity of magnetic field 30

7.2 Periods of data collection 30

7.3 Pseudorapidity range 30

7.4 Number of TPC clusters 31

7.5 Parameters limits and starting values 32

8 Conclusions **38**

Chapter 1

Introduction

1.1 Large Hadron Collider

The Large Hadron Collider (LHC) is the world's largest and highest-energy particle accelerator build by CERN, the European Organisation for Nuclear Research. It lies in a circular tunnel of 27 km in circumference, 50 to 175 meters beneath the Franco-Swiss border near Geneva, Switzerland. The LHC is a synchrotron which accelerates two beams of particles in opposite directions in separate beam pipes. It is designed to accelerate particles to collide with energies at the center of mass up to $\sqrt{s} = 14\ \mathrm{TeV}$ for protons and $\sqrt{s} = 5.52\ \mathrm{TeV}$ for lead ions. There are four main experiments at the LHC: ALICE, ATLAS, CMS, LHCb [1].

ALICE

ALICE (A Large Ion Collider Experiment) is an experiment optimised to study heavy-ion collisions, especially the properties of strongly interacting matter, the phase transition to the Quark-Gluon Plasma and the phase diagram of hadronic matter. It will be described in more details in the next section.

ATLAS

ATLAS (A Toroidal LHC Apparatus) is, together with CMS, one of two general purpose experiments at the LHC. The main goal of this experiment is to search for the Higgs bosons and the origin of mass. It also explores physics beyond the Standard Model e.g. extra dimensions of space, supersymmetry, evidence of the existence of dark matter and dark energy in the Universe.

CMS

CMS (Compact Muon Solenoid), like ATLAS, is a general purpose experiment with similar to ATLAS goals. These two experiments complement each other but are designed and optimised in a different way to ensure cross-check of the measurements.

LHCb

LHCb (Large Hadron Collider beauty) is a specialised experiment, particularly aimed at measuring the parameters of CP (charge conjugation and parity symmetries) violation in the interactions of hadrons composed of beauty hadrons. It investigates the slight difference between matter and antimatter by studying bottom quarks.

1.2 ALICE Experiment

A Large Ion Collider Experiment (ALICE) is a general-purpose detector at LHC aimed to study heavy-ion collisions. It focuses on the physics of strongly interacting matter and the quark-gluon plasma at extreme values of energy density and temperature. The experiment is also designed to study proton-proton and proton-nucleus collisions to provide reference data for the heavy-ion programme and address several specific strong-interaction topics for which ALICE is complementary to the other LHC detectors.

The ALICE detector is composed of 18 different detector systems each with its own specific technology choice and design constraints, driven both by the physics requirements and the experimental conditions expected at LHC. The most unique features of the experiment are tracking and particle identification (PID) over a large momentum range: from few a MeV/c up to over $100\ GeV/c$. This leads to the possibility of studying physics from *soft* (non-perturbative QCD) to *hard* (perturbative QCD, like *jets* and *high-*p_T particle production phenomena).

The experiment is built and is maintained by a collaboration of more than 1000 members from 105 Institutes in 30 countries. Three Polish institutes are involved in the collaboration: Warsaw University of Technology, Andrzej Soltan Institute for Nuclear Studies (from Swierk), and Institute of Nuclear Physics of the Polish Academy of Sciences (from Cracow) [4].

Chapter 2

$\Delta\eta\Delta\phi$ correlation function

$\Delta\eta\Delta\phi$ correlation function is the analysis technique based on the angular distribution of particles created in collision. The final shape of the system in the momentum space is a result of many physical mechanisms that affects the trajectories of the particles. Studying the two-particle correlations in the $\Delta\eta$–$\Delta\phi$ space allows to reveal those mechanisms. The correlation sources, observables and the construction of the $\Delta\eta\Delta\phi$ correlation function will be described in this chapter.

2.1 Observables

Pseudorapidity η

Rapidity is a popular quantity in relativistic physics used alternatively to velocity for measuring motion. In case of particle collisions it is defined relatively to the beam axis as:

$$y = \frac{1}{2} ln \left(\frac{E + p_L c}{E + p_L c} \right), \tag{2.1}$$

where p_L is the component of the momentum along the beam axis and E is the energy of a particle.

Pseudorapidity is an angular variable used to approximate the rapidity of a particle when its mass are not known. It is defined as:

$$\eta = -\ln \left[\tan \left(\frac{\theta}{2} \right) \right], \tag{2.2}$$

where θ is the angle between the particle momentum $\mathbf{p}$ and the beam axis.

In terms of momentum the pseudorapidity variable can be written as:

$$\eta = \frac{1}{2} \ln \left(\frac{|\mathbf{p}| + p_L}{|\mathbf{p}| - p_L} \right), \tag{2.3}$$

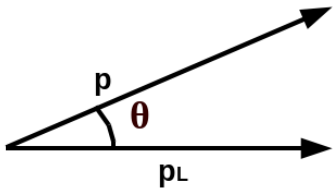

Figure 2.1: Definition of θ angle.

where p_L is the component of the momentum along the beam axis. In relativistic situation when the momentum of a particle is much bigger than its mass ($p >> m$), it is also a good approximation of the rapidity y:

$$y = \frac{1}{2} \ln \left(\frac{E + p_L}{E - p_L} \right). \tag{2.4}$$

One can ask why the η variable is used instead of the angle θ describing the directional distribution of the particles detected after the collision. The reason is that differences in pseudorapidity are Lorentz-invariant under boosts along the beam axis. The difference of pseudorapidity is measured in case of $\Delta\eta\Delta\phi$ correlation function:

$$\Delta\eta = \eta_1 - \eta_2. \tag{2.5}$$

Azimuthal angle ϕ

The azimuthal angle ϕ is the angle between the positive x-axis and the projection of the momentum vector onto the xy-plane (see figure 2.2):

$$\phi = arctan \left(\frac{p_y}{p_x} \right). \tag{2.6}$$

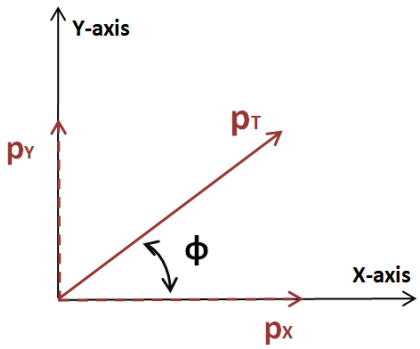

Figure 2.2: The azimuthal angle ϕ definition.

The difference of the azimuthal angle between two particles is defined as:

$$\Delta\phi = (\phi_1 - \phi_2) \, mod 2\pi. \tag{2.7}$$

Such definition of the $\Delta\phi$ variable means that it insensitive to the direction of the coordinate system on the XY plane.

2.2 Construction of $\Delta\eta\Delta\phi$ correlation function

The construction of the $\Delta\eta\Delta\phi$ correlations is based on calculating the difference in pseudo-rapidity η and azimuthal angle ϕ for every pair of particles registered in the detectors after the collision. Then such count fills the two-dimensional histogram with $\Delta\eta$ and $\Delta\phi$ on axes. This procedure is repeated for millions of events run in the same conditions to ensure sufficient statistics. As a result of this analysis we get the *Signal* histogram (see figure 2.3).

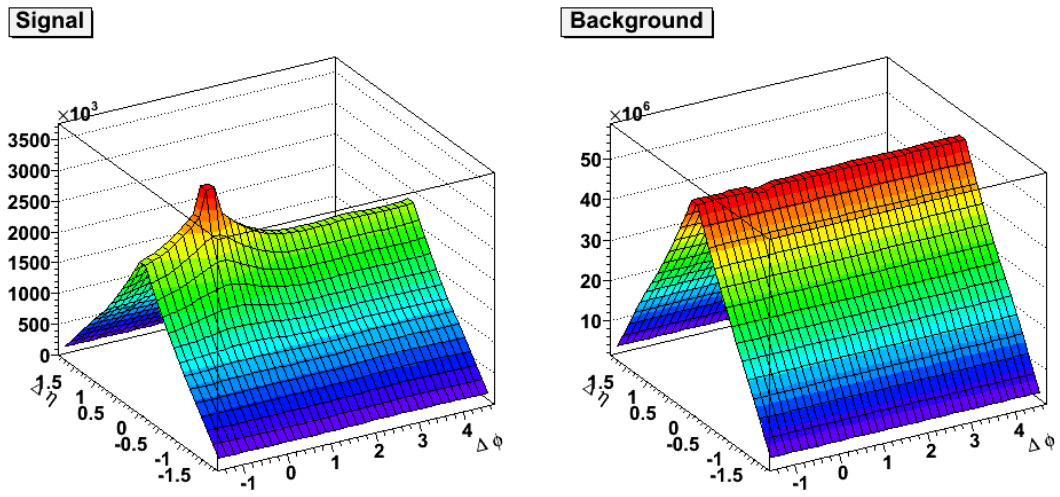

Figure 2.3: The $\Delta\eta\Delta\phi$ *Signal* and *Background* histograms.

The shape of the *Signal* histogram contains not only information about correlations between pairs of particles but also background information coming frome the single particle acceptance. In order to eliminate this background contribution we construct the *Background* histogram. It is build by taking into account pairs of particles coming from different events; so, we expect no physical correlation between them. An example of the *Background* histogram is presented at figure 2.3. Its characteristic triangular shape in variable $\Delta\eta$ is a result of the convolution of two uniform distributions.

Dividing *Signal* by *Background* gives the final shape of the correlation function. Because of the different amount of entries in both histograms it is necessary to scale the *Signal-Background* ratio in the following way:

$$R\left(\Delta\eta,\Delta\phi\right)=\frac{N_{pairs}^{bg}}{N_{pairs}^{sig}}\frac{S\left(\Delta\eta,\Delta\phi\right)}{B\left(\Delta\eta,\Delta\phi\right)}. \tag{2.8}$$

As a result the final, characteristic shape of the $\Delta\eta\Delta\phi$ correlation function is obtained. An example is presented in figure 2.4.

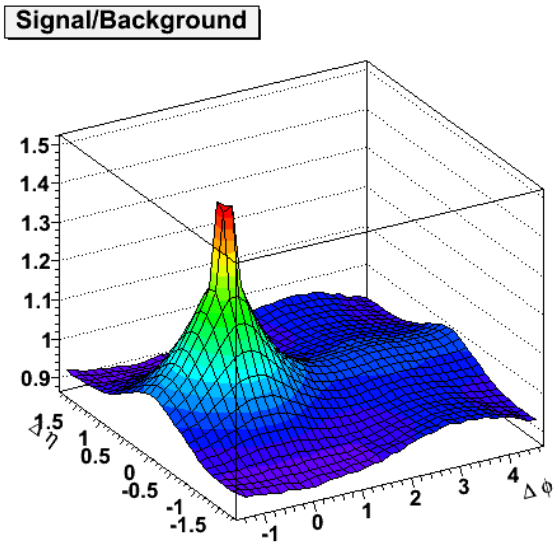

Figure 2.4: The $\Delta\eta\Delta\phi$ correlation function.

2.3 Correlation sources

The $\Delta\eta\Delta\phi$ correlation function is the angular distribution of the trajectories of pairs of particles. Several physical phenomena affect the trajectories of produced particles giving the final shape of the $\Delta\eta\Delta\phi$ correlation. The most important correlation sources are: minijets, Bose-Einstein correlations, elliptic flow, resonance decays and photon conversion. Each of those has an unique structure in $\Delta\eta\Delta\phi$ space which will be shortly described in this section.

Minijets

One can consider minijet as a stream of particles. The most frequent case are the so called *back-to-back* jets – two streams of particles going in opposite directions. There are two possible options, for analysing jets see figure 2.5:

1. Pairs of particles going in the same direction. The difference in angles θ and ϕ is close to 0; so, pairs form a minijet peak are centred at (0,0) – later referred to as the *near-side* peak.

2. Pairs of particles, which go in opposite directions (*back-to-back* jet). The distribution in azimuthal angle ϕ is close to π, but there is no strong correlation in $\Delta\theta$; so, $\Delta\eta$ is almost uniform. As a result we observe a wide ridge at $\Delta\phi = \pi$ – later referred to as *away-side* ridge.

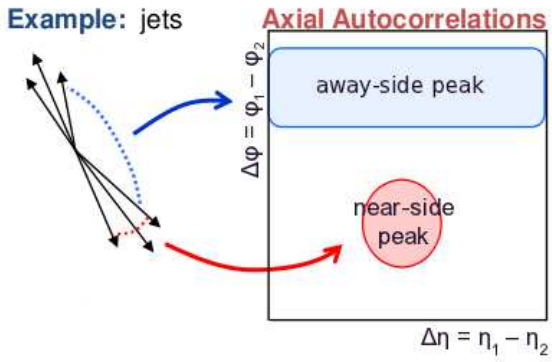

Figure 2.5: The contribution of the minijets to the $\Delta\eta\Delta\phi$ correlation function [5].

Bose-Einstein correlations

According to the Bose–Einstein statistics, identical particles (bosons) are likely to be produced together and emitted in similar direction with small $\Delta\eta$ and $\Delta\phi$. It gives an additional contribution to the *near-side* peak.

Elliptic Flow

In general, the source emitting particles can be anisotropic, which causes correlations among particles. Elliptic flow is a collective effect originating from source anisotropy which adds a $cos(2\Delta\phi)$ type oscillation to the overall shape. It is observed in heavy-ion collision, but not expected in proton-proton collisions.

Resonances

Resonances decay isotropically in their own reference frame. If the decay occurs while moving with certain velocity, all created particles go forward in a similar direction, and with small difference in $\Delta\eta$ and $\Delta\phi$; so, they contribute to the *near-side* peak.

Photon conversion

Electrons and positrons originating from conversion of photons go in the same direction, with small angle differences; therefore, they produce a very sharp *near-side* peak.

Momentum conservation

Conservation laws ensure that for all particles going in similar direction, there would be also a number of particles going in the opposite direction. The momentum conservation law for minijets is actually taken into account in the *near-side* peak *away-side* ridge.

Overall picture

The final shape of the $\Delta\eta\Delta\phi$ correlation function is a mixture of all the above mentioned correlation sources. Figure 2.6 shows all discussed structures referring to the corresponding sources.

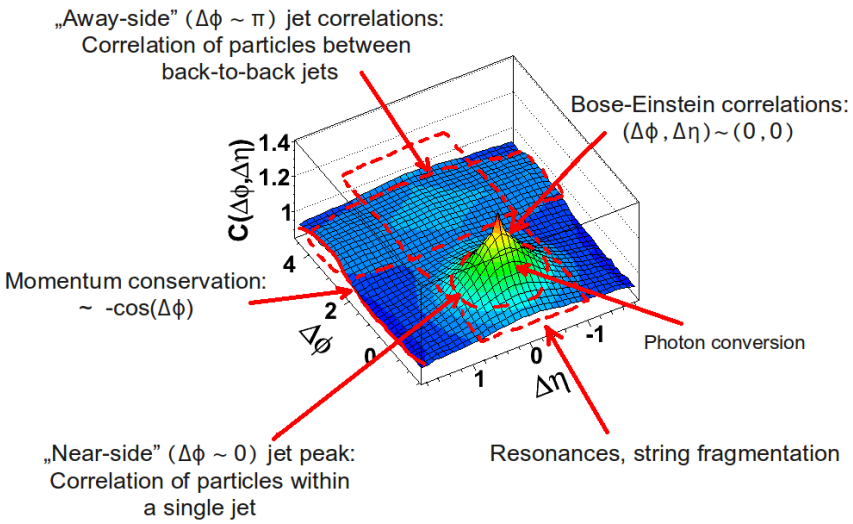

Figure 2.6: Contributions from different correlation sources to the $\Delta\eta\Delta\phi$ correlation function (7 TeV pp collision data).

Chapter 3

Experimental setup and datasets

3.1 Detectors

The $\Delta\eta\Delta\phi$ analysis requires the precise measurement of the production angles of particles. For that purpose three ALICE subsystems were used: Inner Tracking System (ITS), Time Projection Chamber (TPC) and VZERO. The full description of all the ALICE subdetectors can be found in [4].

3.1.1 Inner Tracking System

The Inner Tracking System (ITS) is the innermost subdetector composed of three different types of silicon detectors *Silicon Pixel Detector (SPD)*, *Silicon Drift Detector (SDD)* and *Silicon Strip Detector (SSD)*. The detector layout is shown in figure 3.1.

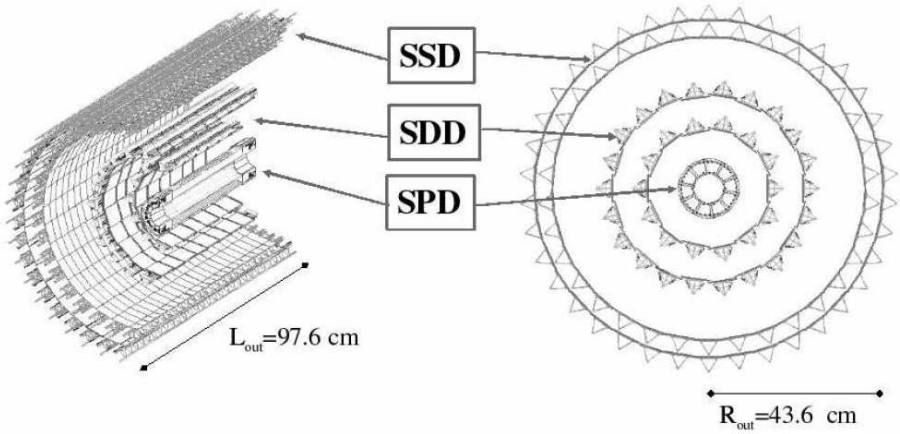

Figure 3.1: The Inner Tracking System [4].

- *Silicon Pixel Detector (SPD)* [3] is essential in determining the position of the primary vertex. It is built of hybrid silicon pixels which consist of silicon detector diodes with

a thickness of $200\ \mu m$. The SPD covers pseudorapidity ranges $|\eta| < 2$ and $|\eta| < 1.4$ for the inner and outer layers respectively, for particles originating from the center of the detector.

- The *Silicon Drift Detector (SDD)* [3] consist of a $300\ \mu m$ thick layer of homogeneous high-resistivity silicon and covers the region $|\eta| < 0.9$. It provides energy-loss information for the particle identification thanks to its analog readout.

- The *Silicon Strip Detector (SSD)* [3] is composed of silicon micro-strips covering $|\eta| < 0.9$. The strips on two sides allow two-dimensional measurements of the track position together with an energy-loss measurement for the particle identification.

3.1.2 Time Projection Chamber

The *Time Projection Chamber (TPC)* [6] is the main tracking detector used to provide information about charged particles; their momenta, vertices positions and particle identification. It is located between radii of $0.85\ m$ and $2.5\ m$ (sensitive volume) and has a length of $5\ m$ – the biggest TPC in the World. The detector is filled with $90\ m^3$ Ne-CO_2-N_2 gas mixture. A drift field of $100\ kV$ stretches between the central electrode (which is located at $z = 0$) and the two readout planes at $z = 2.5\ m$ and $z = -2.5\ m$. A schematic picture of the TPC is shown at figure 3.2.

The readout of the signal is performed by the 570132 pads of 3 different sizes which form the cathode of multi-wire proportional chambers located at the TPC end caps. The end caps are segmented into 18 trapezoidal sectors. These sectors are divided radially in two chambers with varying pad sizes, optimised for the radial dependence of track density. Pads are organised in 159 rows radially.

Tracking particles it the TPC is limited in the pseudorapidity range of $|\eta| < 0.9$ for full radial length and up to $|\eta| < 1.5$ for $1/3$ radial length. The range of transverse momenta at the nominal magnetic field of $0.5\ T$ is from about $200\ MeV/c$ up to $100\ GeV/c$. The momentum resolution of the tracks is better than 2.5% for tracks with a momentum below $4\ GeV/c$.

3.1.3 VZERO

The *VZERO* (also referred to as *V0*) [7] is a small-angle detector consisting of two arrays of 32 scintillator counters, each installed on both sides of the ALICE interaction point: VZERO-A at $z = 3.3\ m$, covering the pseudorapidity range $2.8 < \eta < 5.1$, and VZERO-C at $z = 0.9\ m$, covering the pseudorapidity range $-3.7 < \eta < -1.7$.

The main task of the VZERO system is to provide the online *Level 0* centrality trigger for ALICE by setting a threshold on deposited energy and to provide a background rejection

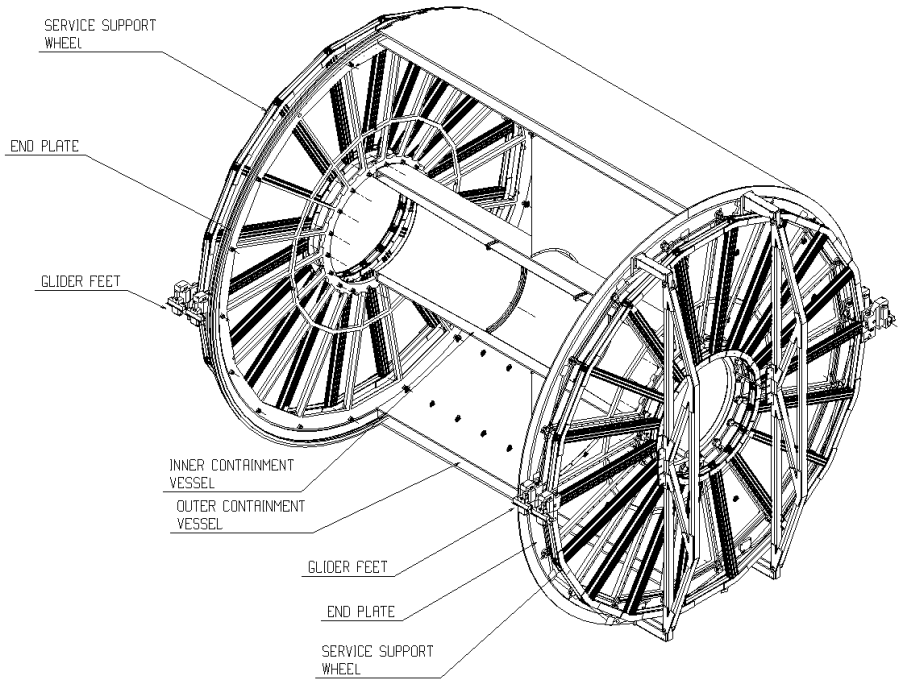

Figure 3.2: The Time Projection Chamber [6].

capability (contribute to the rejection of asymmetric beam-gas events). The time resolution of this detector is better than $1\ ns$. Its response is recorded in a time window of $\pm 25\ ns$ around the nominal beam crossing time.

3.2 Datasets

The data used for this analysis come from the LHC proton-proton runs registered in 2010 and in the first half of 2011 at center of mass energy $\sqrt{s} = 7\ \mathrm{TeV}$. There were 530 millions of analysed events.

3.2.1 Multiplicity ranges

As the multiplicity of the event N_{ch} we consider the total number of measured, charged particles in the detector acceptance range $|\eta| < 1.2$. All the events from the pp collision data at $\sqrt{s} = 7\ \mathrm{TeV}$ were divided into eight multiplicity ranges. The division was made in such way that in each multiplicity range the number of like-sign pairs is comparable. All the ranges are listed in table 3.1. They are also shown in the raw multiplicity distribution plot in figure 3.3.

Range	N_{ch}	$N_{ch}/ < N_{ch} >$	No. events $\times 10^6$
1	2-11	0.15-0.8	322.7
2	12-16	0.9-1.2	85.0
3	17-22	1.2-1.6	61.2
4	23-28	1.7-2.1	37.9
5	29-34	2.2-2.6	17.9
6	35-41	2.7-3.2	8.5
7	42-51	3.2-4.1	3.8
8	52-151	4.2-10.8	0.7

Table 3.1: Multiplicity ranges for pp collision data at the energy of $\sqrt{s} = 7$ TeV.

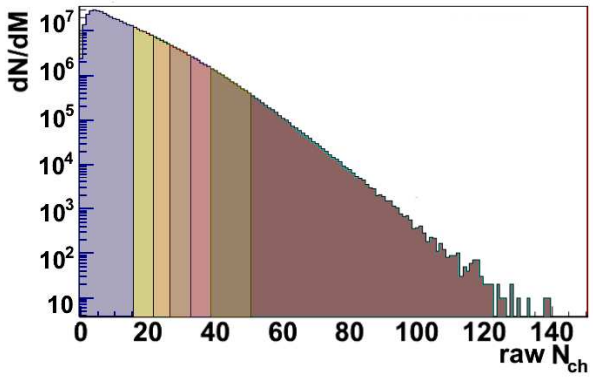

Figure 3.3: Multiplicity distribution for the $\sqrt{s} = 7$ TeV pp collision data with multiplicity ranges in colors.

3.2.2 $p_{T,sum}$ ranges

The quantity related to transverse momentum of the pair of particles is $p_{T,sum}$, defined by the equation:

$$p_{T,sum} = |\mathbf{p_{T,1}}| + |\mathbf{p_{T,2}}|. \tag{3.1}$$

Such definition makes this quantity intensive to the $\Delta\phi$ variable. The introduced $p_{T,sum}$ ranges are presented in table 3.2.2. The p_T,sum distribution plot for the $\sqrt{s} = 7$ TeV data is shown in figure 3.4.

3.2.3 Charge dependence

The analysis was performed on three combination on charge within a pair of particles: positive like-sign (++), negative like-sign (- -), unlike-sign (+-). The difference between like-sign and unlike-sign pairs is expected to be observed at least because of the femtoscopic effects which occur only for identical particles.

Range	p_T-sum $[GeV/c]$
1	0.0-0.75
2	0.75-1.5
3	1.5-2.25
4	2.25-100

Table 3.2: p_T,sum ranges for the $\sqrt{s} = 7$ TeV pp collision data.

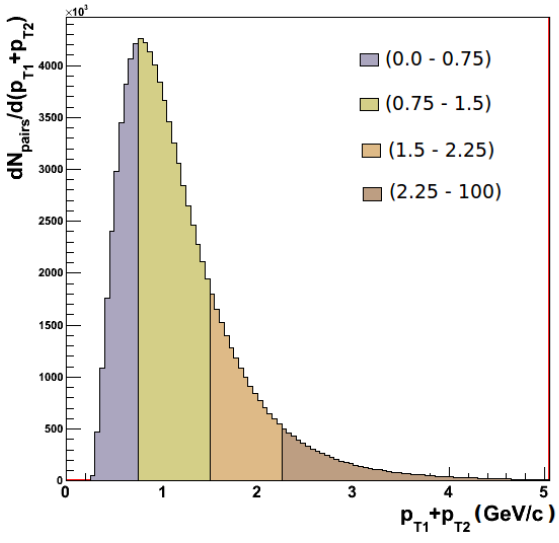

Figure 3.4: $p_{T,sum}$ distribution for the $\sqrt{s} = 7$ TeV pp collision data with $p_{T,sum}$ ranges in colors.

Chapter 4

Fitting procedure

4.1 Introduction

The result of the $\Delta\eta\Delta\phi$ correlation function is a 2D surface in 3D space, with the unique shape which is the result of many physical phenomena that occur just after the collision. In this research we look for an analytical function that describes this shape. Inventing the formula of such function is not an easy task - it has to be relatively simple and contain the minimum number of parameters. Those parameters are generally unknown, but it is possible to obtain them by minimising the difference between experimental correlation function and the analytical function.

Performing the minimisation of the multi-parameter function is, in gerenal, a complicated problem. Even if the theoretical model is constructed well, the analytical function still can have many local minima that are potential solutions of the minimisation process. The physical predictions about parameters help to reach proper solution that fit best to the theory.

In this work fitting the analytical function is based on *MINUIT*, which is a numerical minimisation program originally written in the FORTRAN programming language by the CERN physicist Fred James in the 1970s. Later it was re-written to C++ and adapted to the ROOT environment. The program searches for minima in a user-defined multi-parameter function and analyse the shape of the function around the minimum. The principal application is foreseen for statistical analysis, working on χ-square or log-likelihood functions, to compute the best fit parameter and uncertainties, including correlations between the parameters.

The MINUIT system involves several minimising algorithms. In the case of this work, the MIGRAD method was used.

4.2 MIGRAD algorithm

MIGRAD is a minimisation subroutine based on a variable metric method by Fletcher [8]. It is considered to be the most efficient and complete single method, recommended for general functions. The algorithm is characterised by the following general approach [9]:

1. The vector of parameters $\mathbf{X}$ is filled by starting values given by user. According to those values, the first derivatives $\mathbf{GS}$ are computed. The covariance matrix $\mathbf{V}$ may be only a diagonal matrix or even the unit matrix in the first step.

2. New vector of parameters is computed $\mathbf{X'} = \mathbf{X} - \alpha\mathbf{V}\cdot\mathbf{GS}$, finding the α which minimises the $F(\mathbf{X} - \alpha\mathbf{V}\cdot\mathbf{GS})$. For given $\mathbf{X'}$ the new gradient $\mathbf{GS'}$ is calculated.

3. The covariance matrix $\mathbf{V}$ is updated by the general form $\mathbf{V'} = \mathbf{V} + f(\mathbf{V}, \mathbf{X}, \mathbf{X'}, \mathbf{GS}, \mathbf{GS'})$. Then $\mathbf{GS}$ is replaced by $\mathbf{GS'}$, $\mathbf{X}$ by $\mathbf{X'}$, and $\mathbf{V}$ by $\mathbf{V'}$ and steps (1) and (2) are repeated until some convergence criteria are satisfied.

The "estimated distance to minimum" (EDM) is used as the convergence criteria. It is calculated by:

$$EDS = \mathbf{GS}^T \cdot \mathbf{V} \cdot \mathbf{GS}. \tag{4.1}$$

4.3 Chi-square function

Minimising algorithm works on the χ^2, defined by:

$$\chi^2(\mathbf{X}) = c\sum_{i=1}^{n}(f(\Delta\eta_i, \Delta\phi_i, \mathbf{X}) - \epsilon_i)^2, \tag{4.2}$$

where f is a user-defined multi-parameter fitting function, ϵ_i is the measured value and X is the vector of free parameters being fitted. As a result of the minimisation of the χ^2 value we obtain the parameters that describe the dataset best.

4.4 Residual histogram

Because the analytical function used for fitting is unknown, we need a tool to check and improve many of the proposed functions. Using only the χ-square value is insufficient – it indicates only if the fitting is correct or not without any insight on possible better solutions. For that reason the *Residual histogram* is used. The data of the $\Delta\eta\Delta\phi$ correlation function are stored in two-dimensional histogram (ROOT's *TH2D* object). According to the used fitting function and obtained parameters the corresponding *Fitted histogram* is created. The *Residual histogram* is a difference between them and is graphically displayed in order to indicate the improvements in the fitting function. The fitting is correct if a flat *Residual histogram* is obtained.

4.5 Fitting formula

In chapter 2 three main structures in the shape of the $\Delta\eta\Delta\phi$ correlation function are distinguished: *near-side* peak, *away-side* ridge and *longitudinal* ridge. Fitting formula is intended to reproduce all those structures.

4.5.1 The combination of the Gaussian functions

The first attempt on finding the right fitting function was to use the combination of the Gaussian functions. See equation 4.3.

$$\begin{aligned} C(\Delta\phi,\Delta\eta) &= M_M \exp\left(-\left(\frac{\Delta\phi^2}{2\sigma_{M\phi}^2}+\frac{\Delta\eta^2}{2\sigma_{M\eta}^2}\right)\right) + M_M \exp\left(-\left(\frac{(\Delta\phi-2\pi)^2}{2\sigma_{M\phi}^2}+\frac{\Delta\eta^2}{2\sigma_{M\eta}^2}\right)\right) \\ &+ M_S \exp\left(-\left(\frac{\Delta\phi^2}{2\sigma_{S\phi}^2}+\frac{\Delta\eta^2}{2\sigma_{S\eta}^2}\right)\right) \\ &+ M_A \exp\left(-\left(\frac{(\Delta\phi-\pi)^2}{2\sigma_{A\phi}^2}\right)\right) + M_A \exp\left(-\left(\frac{(\Delta\phi+\pi)^2}{2\sigma_{A\phi}^2}\right)\right) \\ &+ M_L \exp\left(-\left(\frac{\Delta\eta^2}{2\sigma_{L\eta}^2}\right)\right) \\ &+ N, \end{aligned} \tag{4.3}$$

where M_M, $\sigma_{M\phi}$ and $\sigma_{M\eta}$ are parameters of the *near-side* Gaussian, meant to describe the minijet correlation structure, M_S, $\sigma_{S\phi}$ and $\sigma_{S\eta}$ are meant to describe the *near-side* femtoscopic correlations, M_A and $\sigma_{A\phi}$ are meant to describe the *away-side* ridge and momentum conservation, and M_L, $\sigma_{L\eta}$ are meant to describe the longitudinal ridge. In addition, N is the overall normalisation. The $\Delta\phi$ variable refers to the diffenerce in the polar angle which is periodic, so all the components of the function with the $\Delta\phi$ variable also have to be periodic with period 2π.

Figure 4.1 shows the visualisation of data correlation function, the fitted function and the residual histogram. The structures in residual histogram prove that proposed formula does not fit to the data well. The radial shape around the point (0,0) suggest that the *near-side* peak in the data correlation function has different slope than result of the fitting function. It means that the formula require some modification of the shape.

4.5.2 The combination of the modified Gaussian functions

The shape of the Gaussian functions was modified by additional exponents to ensure better fit to the data. See the new fitting formula on equation 4.4.

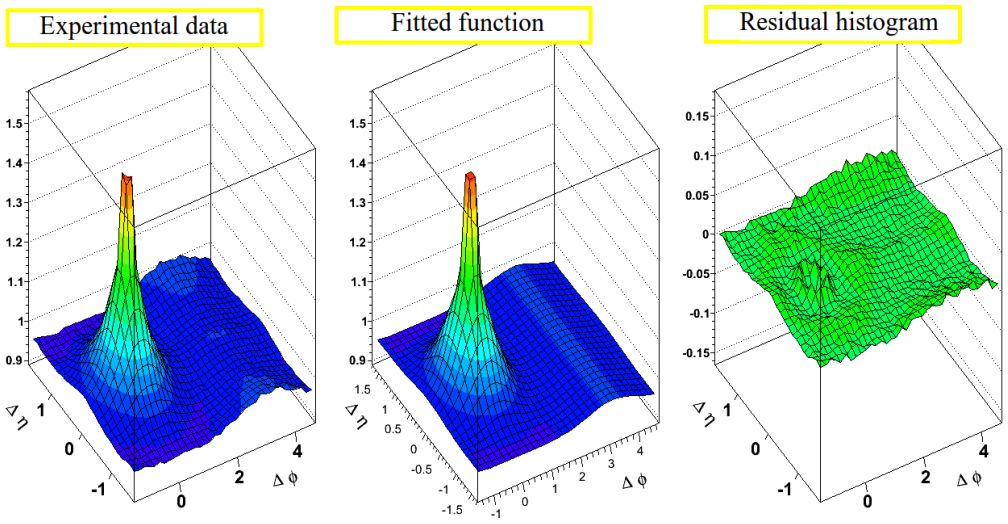

Figure 4.1: The example of results for function 4.3.

$$
\begin{aligned}
C(\Delta\phi,\Delta\eta) &= M_M \exp\left(-\left(\frac{\Delta\phi^2}{2\sigma^2_{M\phi}}+\frac{\Delta\eta^2}{2\sigma^2_{M\eta}}\right)^{e_M}\right) + M_M \exp\left(-\left(\frac{(\Delta\phi-2\pi)^2}{2\sigma^2_{M\phi}}+\frac{\Delta\eta^2}{2\sigma^2_{M\eta}}\right)^{e_M}\right) \\
&+ M_S \exp\left(-\left(\frac{\Delta\phi^2}{2\sigma^2_{S\phi}}+\frac{\Delta\eta^2}{2\sigma^2_{S\eta}}\right)\right) \\
&+ M_A \exp\left(-\left(\frac{(\Delta\phi-\pi)^2}{2\sigma^2_{A\phi}}\right)^{e_A}\right) + M_A \exp\left(-\left(\frac{(\Delta\phi+\pi)^2}{2\sigma^2_{A\phi}}\right)^{e_A}\right) \\
&+ M_L \exp\left(-\left(\frac{\Delta\eta^2}{2\sigma^2_{L\eta}}\right)^{e_L}\right) \\
&+ N, \qquad (4.4)
\end{aligned}
$$

where e_M, e_A and e_L are the additional exponents that modify the Gaussian functions. The rest of the parameters is consistent with equation 4.3. The influence of the exponent on the shape of Gaussian function is shown in figure 4.2. Further studies proved that modification is necessary only in case of the minijet peak, the other exponents are fixed to 1.

Figure 4.3 proves that the modified Gaussian functions correspond to the data much better than it was in the previous case. The residual histogram is almost flat, except of the ”wings” structure in the large $\Delta\eta$ region. The simulations have shown that its shape differs with cuts proceeded on data. It indicates that those ”wings” are a result of detector acceptance effects.

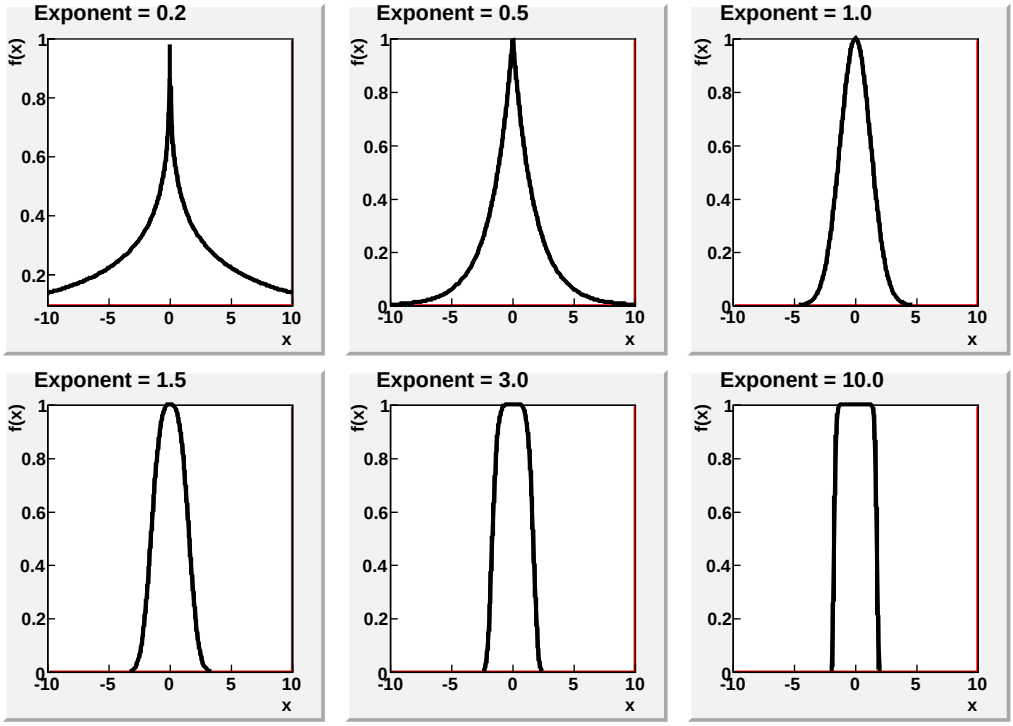

Figure 4.2: The influence of exponent on the shape of the Gaussian function.

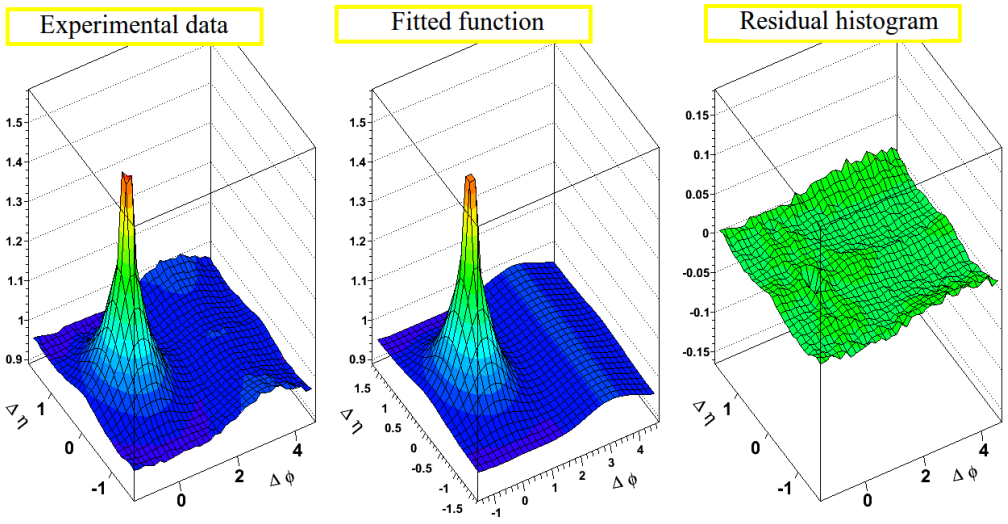

Figure 4.3: The example of results for function 4.4.

4.5.3 The combination of the modified Gaussian functions with the second order polynomial function

The wing structures were accounted for by adding the second order polynomial function to the fitting formula, which is given on equation 4.5.

$$
\begin{aligned}
C(\Delta\phi,\Delta\eta) &= M_M \exp\left(-\left(\frac{\Delta\phi^2}{2\sigma^2_{M\phi}}+\frac{\Delta\eta^2}{2\sigma^2_{M\eta}}\right)^{e_M}\right)+M_M\exp\left(-\left(\frac{(\Delta\phi-2\pi)^2}{2\sigma^2_{M\phi}}+\frac{\Delta\eta^2}{2\sigma^2_{M\eta}}\right)^{e_M}\right)\\
&+ M_S\exp\left(-\left(\frac{\Delta\phi^2}{2\sigma^2_{S\phi}}+\frac{\Delta\eta^2}{2\sigma^2_{S\eta}}\right)\right)\\
&+ M_A\exp\left(-\left(\frac{(\Delta\phi-\pi)^2}{2\sigma^2_{A\phi}}\right)\right)+M_A\exp\left(-\left(\frac{(\Delta\phi+\pi)^2}{2\sigma^2_{A\phi}}\right)\right)\\
&+ M_L\exp\left(-\left(\frac{\Delta\eta^2}{2\sigma^2_{L\eta}}\right)\right)\\
&+ P\left(\Delta\eta^2\right)+N, \qquad (4.5)
\end{aligned}
$$

where P is the parameter of the second order polynomial function. The formula 4.5 is the final stage of obtaining the correct fitting function, which is proved on figure 4.4.

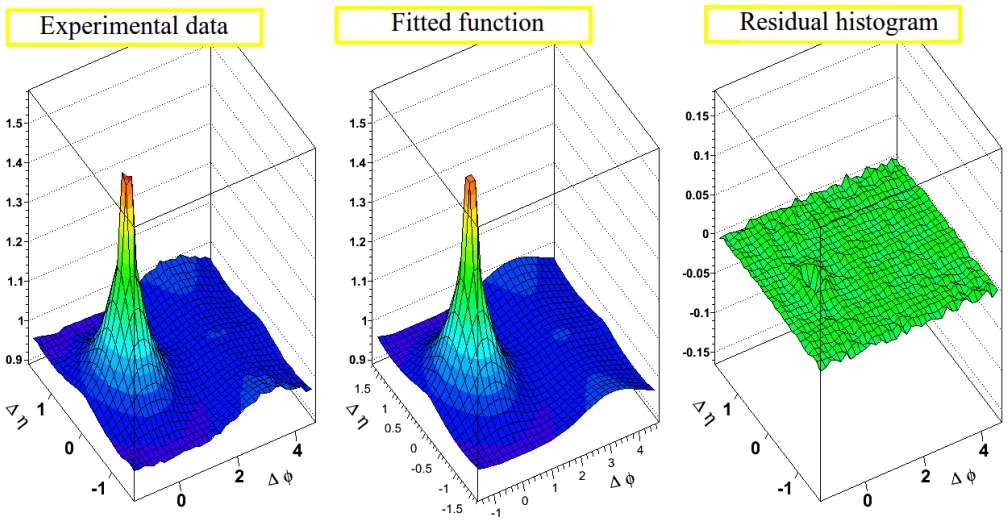

Figure 4.4: The example of results for function 4.5.

Chapter 5

Developed software tools

In this chapter the program used for fitting the experimental $\Delta\eta\Delta\phi$ correlation function is shortly described. It was written in the ROOT environment [2] and is based on the two methods: `fit(TH2D*)` and `fitppmb(int)`.

Format of the experimental data

The experimental data come from the analysis done by Malgorzata Janik and Lukasz Graczykowski. The histograms (`TH2D` objects) with the *signal* and *background* (see chapter 2) data of the $\Delta\eta\Delta\phi$ correlation function for each multiplicity and $p_{T,sum}$ case are stored in the `.root` file. Reading form the `.root` file and creating the final correlation function is performed in the method `fitppmb(int)`.

The fitppmb(int) method

This is the main method which is intended to perform the following tasks:

- read the *signal* and *background* histograms from the `.root` file,
- create the histogram with the $\Delta\eta\Delta\phi$ correlation function,
- act the `fit(TH2D*)` method on the histogram with the $\Delta\eta\Delta\phi$ correlation function,
- write the results to the `.root` file.

Creating the $\Delta\eta\Delta\phi$ correlation function

The argument of the `fitppmb(int)` method is used to choose the charge of particles within a pair. There are three possibilities: both particles are positively charged (plus), both particles are negatively charged (minus) and pairs of particles with opposite charge (mixed).

```
switch(namech){
case 0: name = "plus"; break;
case 1: name = "minus"; break;
case 2: name = "mixed"; break;
}
```

Then the data is read from the proper `.root` file. The final $\Delta\eta\Delta\phi$ correlation function is obtained by dividing *signal* by *background* and performing the scaling, which is necessary because of different number of entries in *signal* and *background* histograms.

```
double scale_den=((TH2D*)gDirectory->Get(Signal)->Integral();
double scale_num=((TH2D*)gDirectory->Get(Background)->Integral();
TH2D* num = (TH2D*)gDirectory->Get(Signal);
num->Divide((TH2D*)gDirectory->Get(Background));
num->Scale(scale_den/scale_num);
```

After creating the `num` histogram with the $\Delta\eta\Delta\phi$ correlation function the `fit(TH2D*)` method is run.

```
fit(num);
```

The last task of the `fitppmb(int)` method is to create the plots (`TH1D` objects) of parameters which are the result of the `fit(TH2D*)` method and save them to the `.root` file.

```
TFile *out = new TFile(Form("out.fit.%s.root",name),"RECREATE");
out->cd();

hNormalization->Write();
hMinijetPeakMagnitude->Write();
hMinijetPeakPhi->Write();
hMinijetPeakEta->Write();
hMinijetPeakExp->Write();
hSharpPeakMagnitude->Write();
hSharpPeakPhi->Write();
hSharpPeakEta->Write();
hAwaySideMagnitude->Write();
hAwaySidePhi->Write();
hAwaySideExp->Write();
hLongRidgeMagnitude->Write();
hLongRidgeEta->Write();
hLongRidgeExp->Write();
hParabola->Write();
```

The fit(TH2D*) method

This method is intended to perform the fitting of the analytical function (TF2 object) to the $\Delta\eta\Delta\phi$ correlation function. At first, it creates the fitting function according to the formula 4.5.

```
const char *form = "[0]
+ [1]*exp(-TMath::Power(((x-PI)*(x-PI))/(2*[10]*[10]),[12]))
+ [1]*exp(-TMath::Power(((x+PI)*(x+PI))/(2*[10]*[10]),[12]))
+ [2]*exp(-TMath::Power(x*x/([3]*[3]*2)+y*y/([4]*[4]*2),[13]))
+ [2]*exp(-TMath::Power((x-2PI)*(x-2PI)/([3]*[3]*2)
                        + y*y/([4]*[4]*2),[13]))
+ [5]*exp(-(x*x)/(2*[6]*[6])-(y*y)/(2*[7]*[7]))
+ [8]*exp(-TMath::Power(y*y/(2*[9]*[9]),[11]))
+ [14]*y*y";

fitfun = new TF2("fitfun",form);
```

Then the starting values of parameters and limits are defined.

```
// Minijet
fitfun->SetParameter(2, 0.4);
fitfun->SetParameter(3, 0.7);
fitfun->SetParameter(4, 0.40);
fitfun->SetParameter(13,0.6);
// Sharp peak
fitfun->SetParameter(5, 0.5);
fitfun->SetParameter(6, 0.11);
fitfun->SetParameter(7, 0.17);
// Long ridge
fitfun->SetParameter(8, 0.01);
fitfun->SetParameter(9, 0.8);
fitfun->SetParameter(11, 1.0);
// Away-side ridge
fitfun->SetParameter(1, 0.08);
fitfun->SetParameter(10, 1.0);
fitfun->FixParameter(12, 1.0);
// Parabola
fitfun->SetParameter(14, 0.0);
// Limits
```

```
fitfun->SetParLimits(0, 0.60, 1.02);
fitfun->SetParLimits(3, 0.1, 0.8);
fitfun->SetParLimits(4, 0.1, 1.0);
fitfun->SetParLimits(13, 0.35, 0.75);
fitfun->SetParLimits(5,0.1, 10.0);
fitfun->SetParLimits(6,0.1, 0.3);
fitfun->SetParLimits(7,0.1, 0.3);
fitfun->SetParLimits(8, 0.0, 100.0);
fitfun->SetParLimits(9, 0.4, 2.55);
fitfun->SetParLimits(11, 0.0, 1.5);
fitfun->SetParLimits(1, 0.0, 100.0);
fitfun->SetParLimits(10, 0.6, 3.0);
```

The next step is to run the *MINUIT* algorithm which looks for the optimum values of the parameters.

```
inhist->Fit(fitfun,"WIRN","");
```

`WIRN` are the options of the fit:

- ”W” Set all errors to 1
- ”I” Use integral of function in bin instead of value at bin center
- ”R” Use the range specified in the function range
- ”N” Do not store the graphics function, do not draw

The last task of this method is to create the residual histogram.

```
for (int ix=1; ix<=res->GetNbinsX(); ix++)
  for (int iy=1; iy<=res->GetNbinsY(); iy++){
    vh = inhist->GetBinContent(ix, iy);
    vf = fitfun->Eval(inhist->GetXaxis()->GetBinCenter(ix),
      inhist->GetYaxis()->GetBinCenter(iy));
    res->SetBinContent(ix, iy, vh-vf);
  }
```

At the end the fitted function and the residual histogram are written to the proper `.root` file.

```
canfit->SaveAs(Form("canfit.%s.root",inhist->GetTitle()),"RECREATE");
```

The figures 4.1, 4.3, 4.4 and all the figures in the chapter 6 are obtained by described in this chapter software tools and stored in the `.root` files.

Chapter 6

Fitting results

The parameters of the fit are visualy presented in the plots in the multiplicity and transverse momentum dependence. They are shown together with the plots of the $\Delta\eta\Delta\phi$ correlation functions in order to easily associate fit results with general trends in the data. In a few situations, when the structures of the correlation functions are very small, the parameters reach the values near to zero which causes enormously high error bars. Symbols on plots correspond to the symbols of fitting formula 4.5, we repeat:

- M_M, $\sigma_{M\phi}$, $\sigma_{M\eta}$, e_M – parameters of minijet peak,
- M_S, $\sigma_{S\phi}$, $\sigma_{S\eta}$ – parameters of peak describing femtoscopic effects,
- M_A, $\sigma_{A\phi}$, e_A – parameters of away-side ridge,
- M_L, $\sigma_{L\eta}$, e_L – parameters of longitudinal ridge,
- P – parabola parameter,
- N – normalisation.

In legend:

- ”plus” means pairs of positively charged particles,
- ”minus” means pairs of negatively charged particles,
- ”unlike-sign” means pairs with particles of opposite charge.

6.1 Multiplicity dependence of the fit parameters

In this chapter the multiplicity of the event is represented as a root of the third degree of a number of detected charged particles per the unit of pseudorapidity. Further it will be simply called multiplicity.

Energy $\sqrt{s} = 7\ TeV$

Observations, figure 6.1:

- Minijet peak has the same magnitude for like and unlike-sign pairs, but is wider for unlike-sign. Exponent is much lower than 1, which makes the peak more sharp than non-modified Gaussian,
- Away-side ridge for unlike-sign pairs is a bit bigger than for like-sign pairs, which is consistent with the message of minijet near-side peak (because minijet peak should be related with away-side ridge),
- Longitudinal ridge exist only for lowest multiplicity and unlike-sign particles,
- Femtoscopic effects are included only in case of like-sign pairs and are lowering with multiplicity,
- "Wings", which we relate with acceptance effects, are lowering with multiplicity,
- Near-side peak for negatively charged pairs is higher than for positively charged pairs.

6.2 Transverse momentum dependence of the fit parameters

The shape of correlation function varies significantly in $p_{T,sum}$ dependence, especially for low $p_{T,sum}$. This section involves plots describing this variation. Most significant in this investigation is the relation between minijets and Bose-Einstein effects, which are expected to be easy to disentangle in those circumstances.

Energy $\sqrt{s} = 7\ TeV$

Observations, figure 6.2:

- big difference between like-sign and unlike-sign especially for low $p_{T,sum}$. It is associated with femtoscopic effects expected for like-sign pairs,
- femtoscopic effects lowering with $p_{T,sum}$ for like-sign pairs,
- minijet peak and away-side ridge rising with $p_{T,sum}$ both for like-sign and unlike-sign pairs,
- small longitudinal ridge observed only for low $p_{T,sum}$,
- negligible "wings" effects.

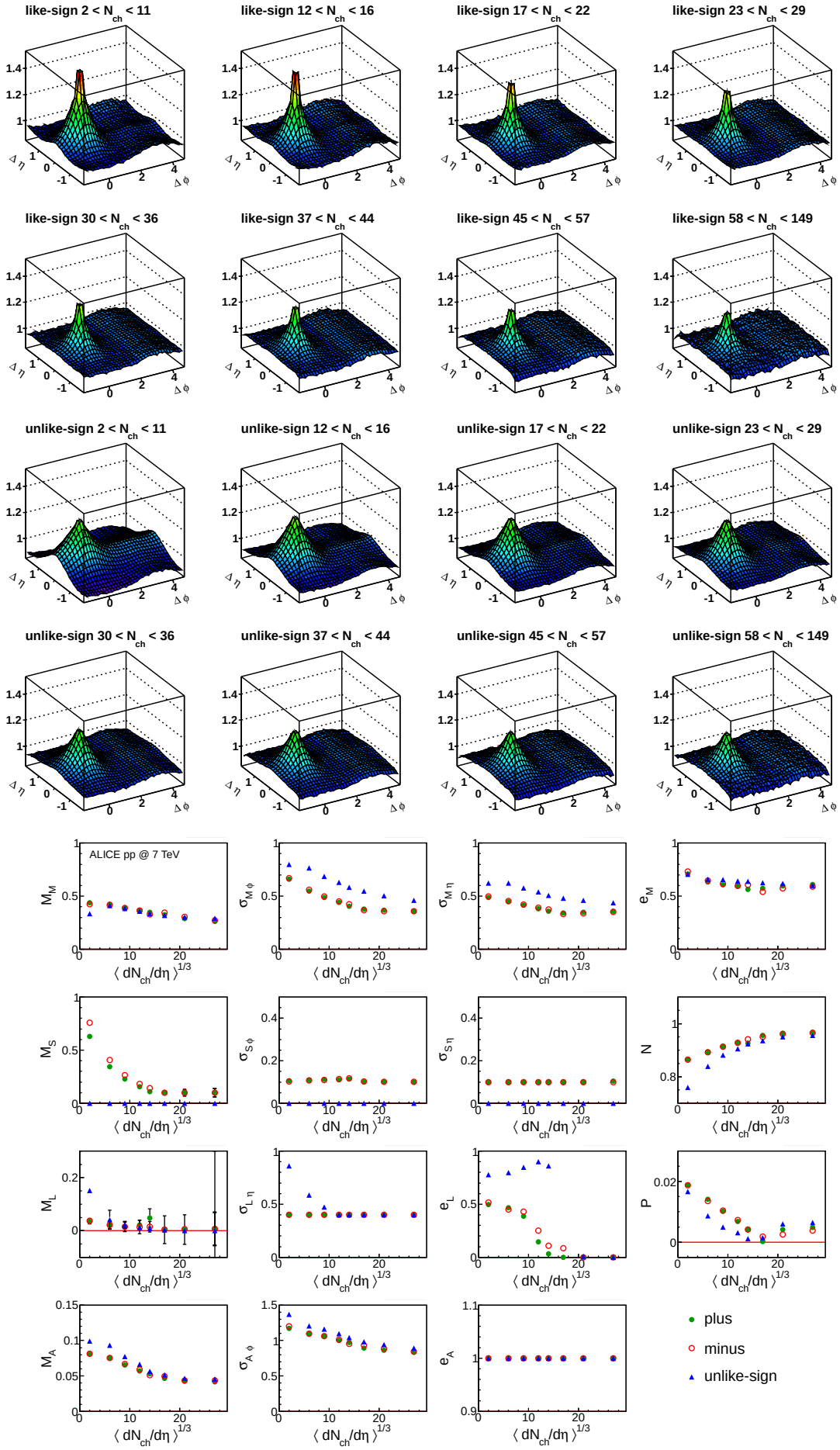

Figure 6.1: Multiplicity dependence at $\sqrt{s} = 7$ TeV.

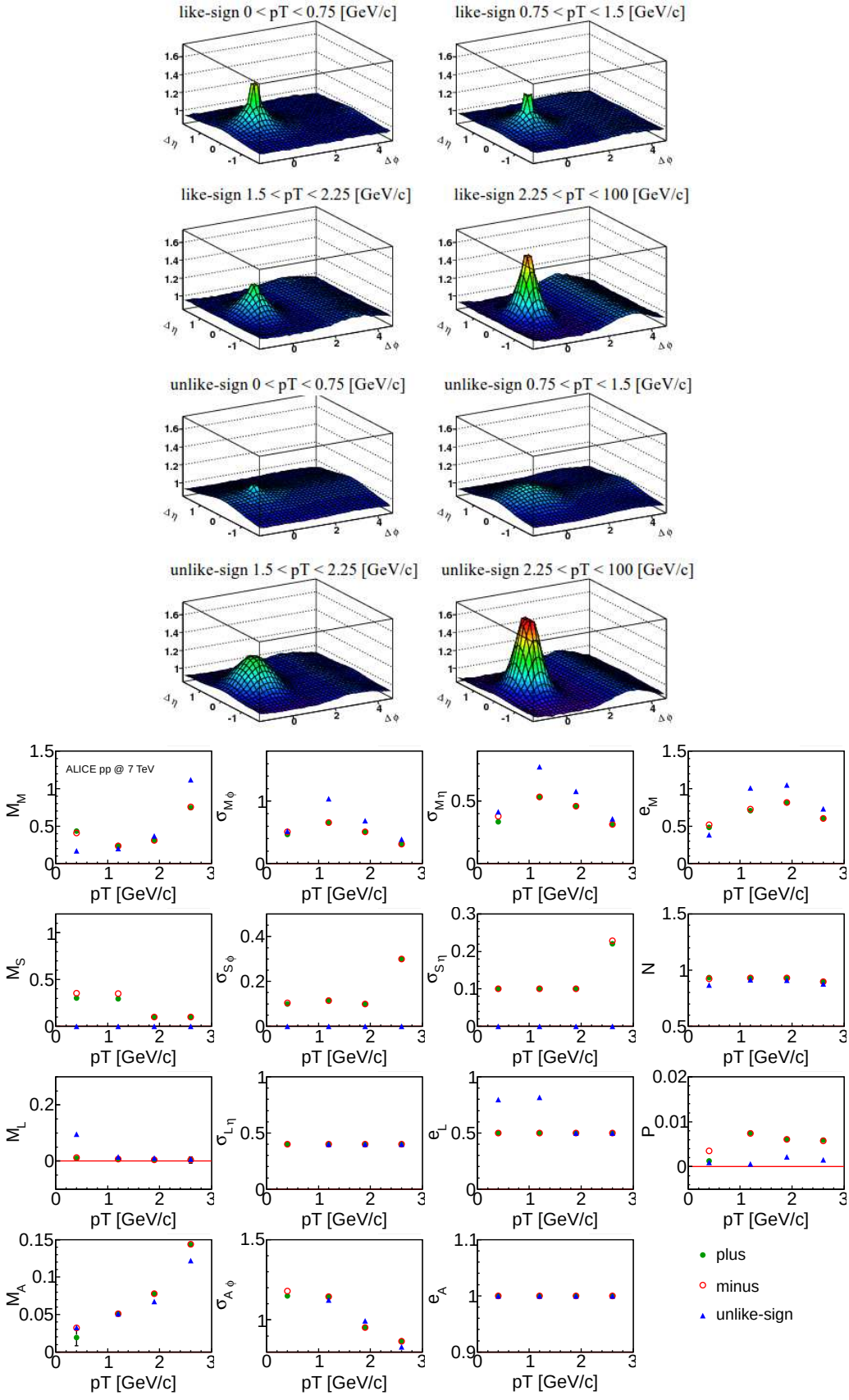

Figure 6.2: $p_{T,sum}$ dependence at $\sqrt{s} = 7$ TeV.

Chapter 7

Analysis of uncertainties

This chapter presents the analysis of uncertainties by studying many sources of the systematic errors.

7.1 Polarity of magnetic field

Magnetic field fills the detector in order to bend the trajectories of particles. Generally it is one direction of magnetic field and two possible senses, opposite to each other. In the ideal detector observables should not depend on the sense of magnetic field. However, if we consider additional influences e.g. external magnetic field or detector response, then some variation may be observed. The results of this investigation are shown in figure 7.1. The difference between the fit values for opposite senses of magnetic field is a contribution to the systematic error.

7.2 Periods of data collection

LHC is a long term project; so, stability of the detectors is a very important factor. A comparison of the fit parameters coming from different periods of data collection has been done to investigate the time variation of the results. According to the results shown in figures 7.2 there is no time dependence of the fit parameters and the only difference comes from different senses of the magnetic field.

7.3 Pseudorapidity range

The detectors used in the experiment, and especially the TPC which is the most important in $\Delta\eta\Delta\phi$, cover limited range of pseudorapidity. For $|\eta| > 1.5$ new structures appear so called "wings effect" which may affect fit the parameters. To check this influence the fitting procedure was performed on data with different pseudorapidity ranges and it turn out that there is no

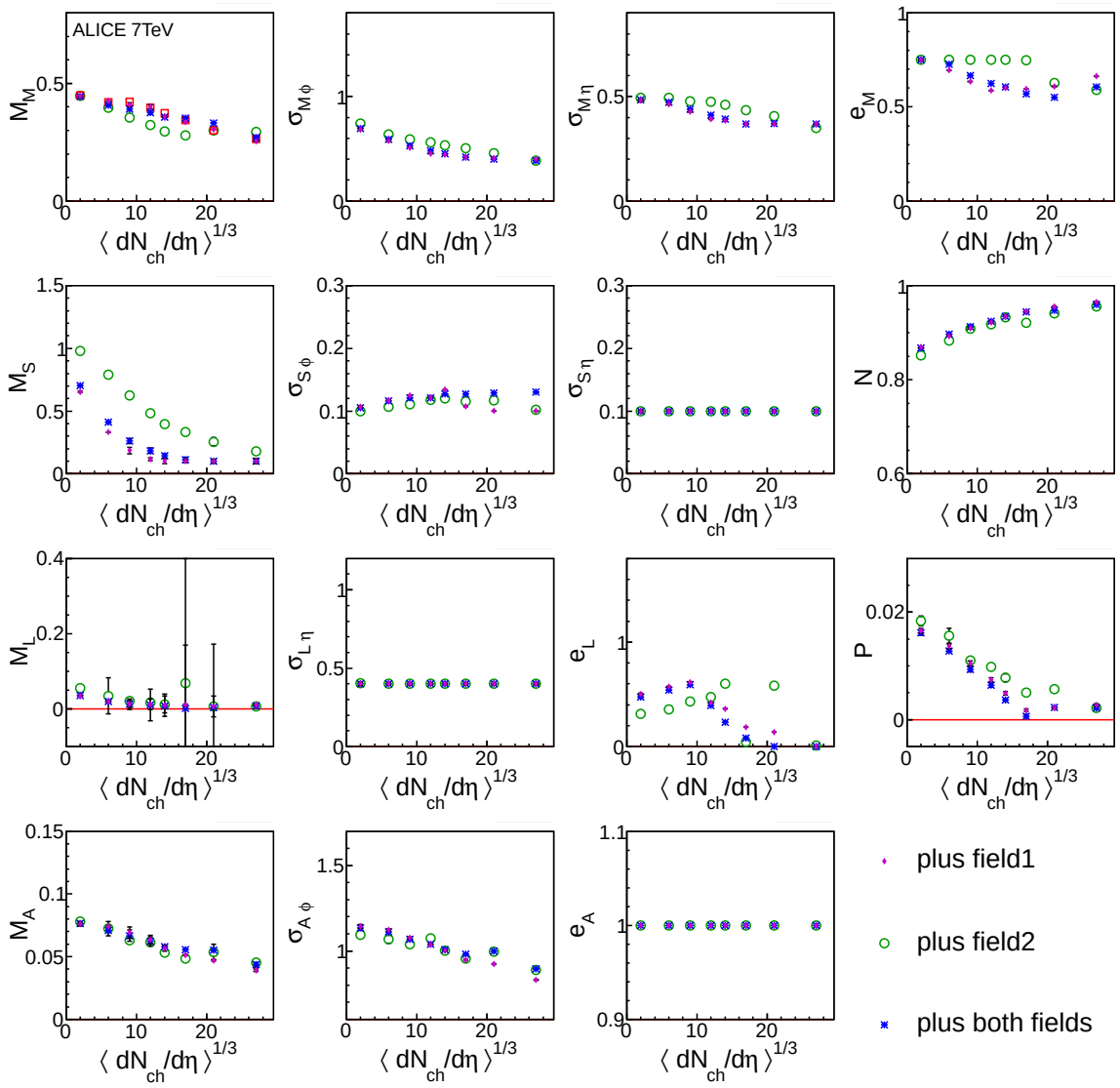

Figure 7.1: Comparison of fit parameters for both senses of magnetic field and overall data.

influence on fit parameters in the investigated pseudorapidity ranges. The results are shown in figures 7.3 and 7.4.

7.4 Number of TPC clusters

The minimum number of TPC clusters associated to the track was set to 70 (maximal value of the associated clusters is 159, which is related to the total number of padrows in the TPC detector). We studied the influence of changing this setup to 60 and 80 to observe the variation of fit parameters. Plots on figure 7.5 show that there is no significant influence.

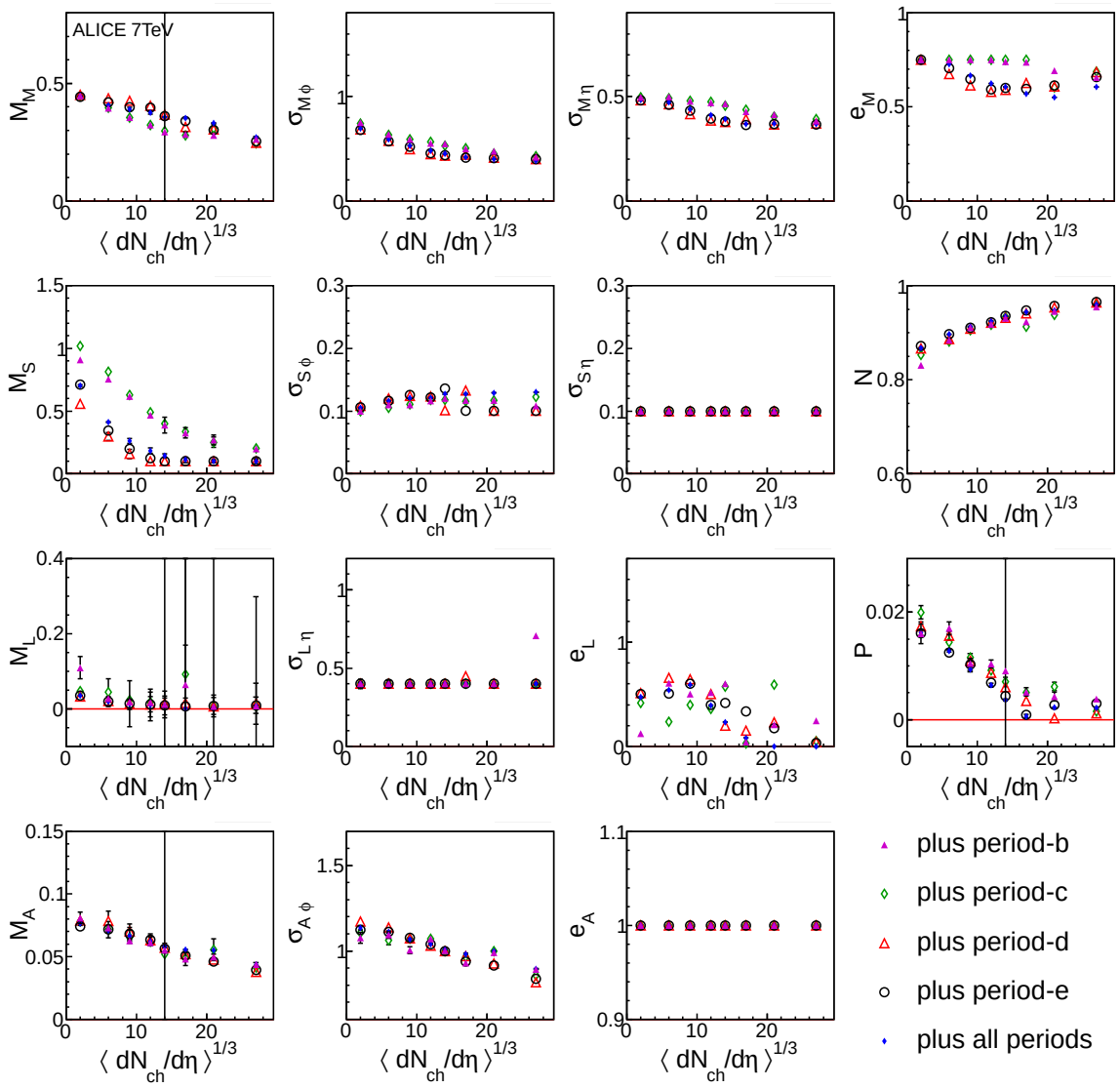

Figure 7.2: Comparison of fit parameters for different periods and like-sign pair particles.

7.5 Parameters limits and starting values

Depending on different starting parameters and parameters limits the result of the fit may vary. The reason is that the chi-square function, which is minimised in order to get the best fit, may have several local minima (fit solutions). The multi-dimensional space of parameters has regions leading to different solutions so it is essential to choose the right starting parameters. Limits are necessary to avoid mathematically correct, but physically meaningless solutions. The expectation for the a correct solution is that small changes of the starting parameters and limits will not affect the final result of the fit. The small difference in result of the parameters is considered as a contribution to the statistical errors.

Figures 7.6 and 7.7 show that the solution is stable – 10% change of starting parameters and limits generally does not affect the final fit parameters.

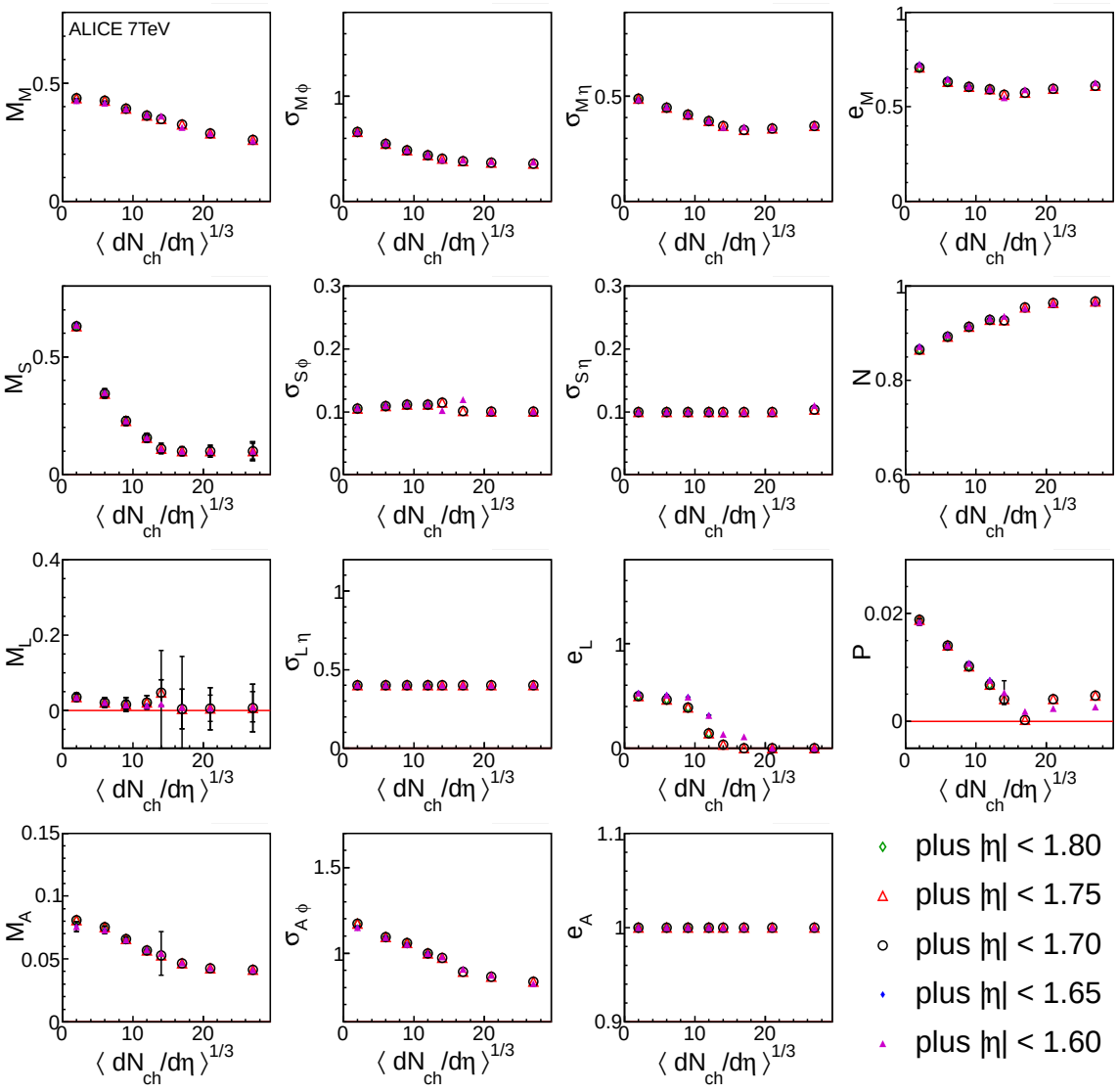

Figure 7.3: Comparison of fit parameters for different η ranges and like-sign pair particles.

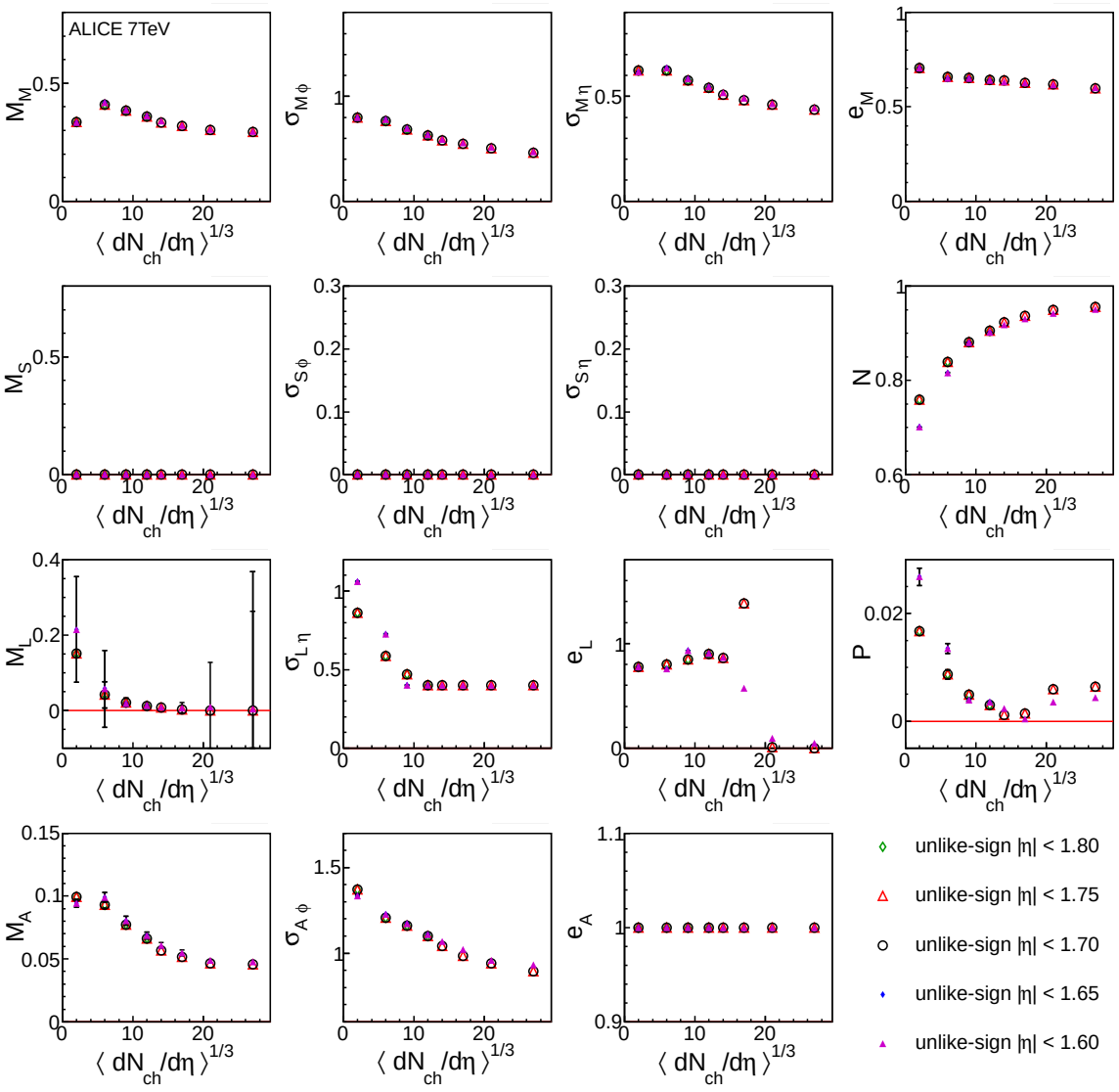

Figure 7.4: Comparison of fit parameters for different η ranges and unlike-sign pair particles.

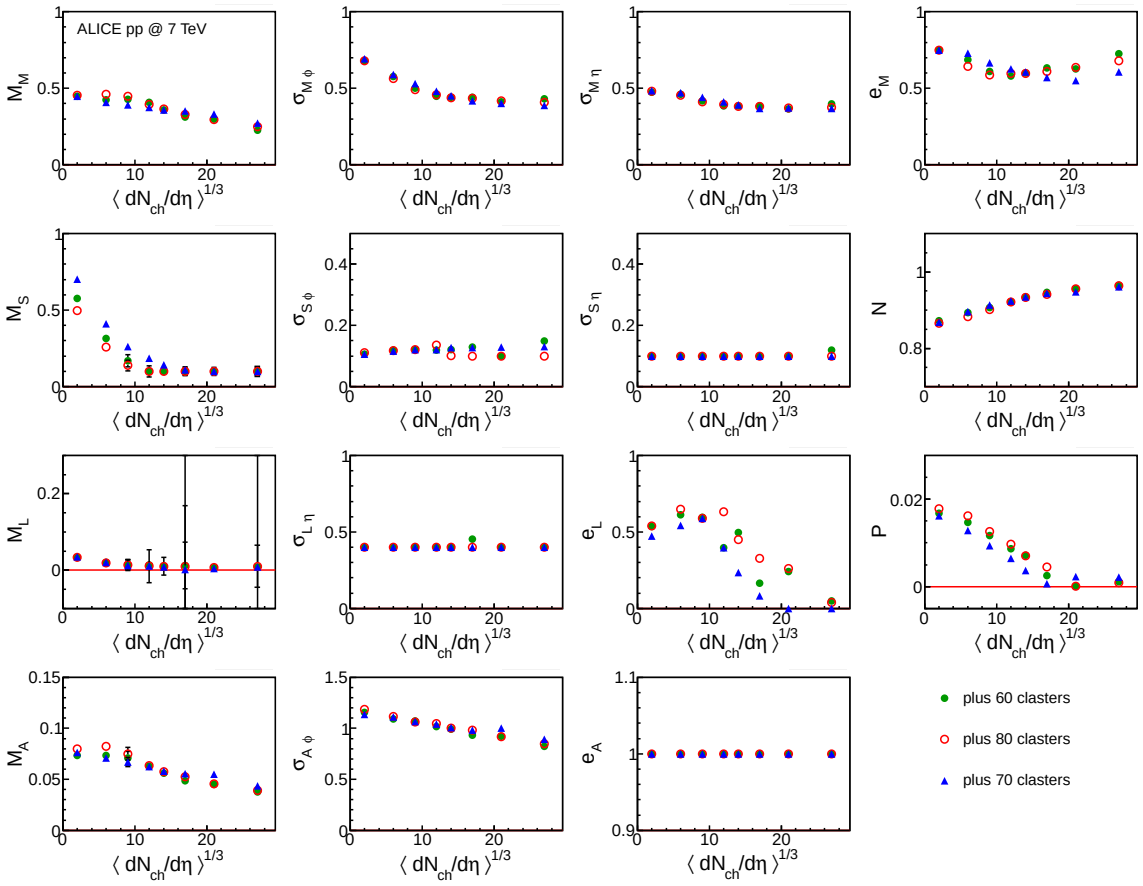

Figure 7.5: Comparison of fit parameters for different number of TPC clusters.

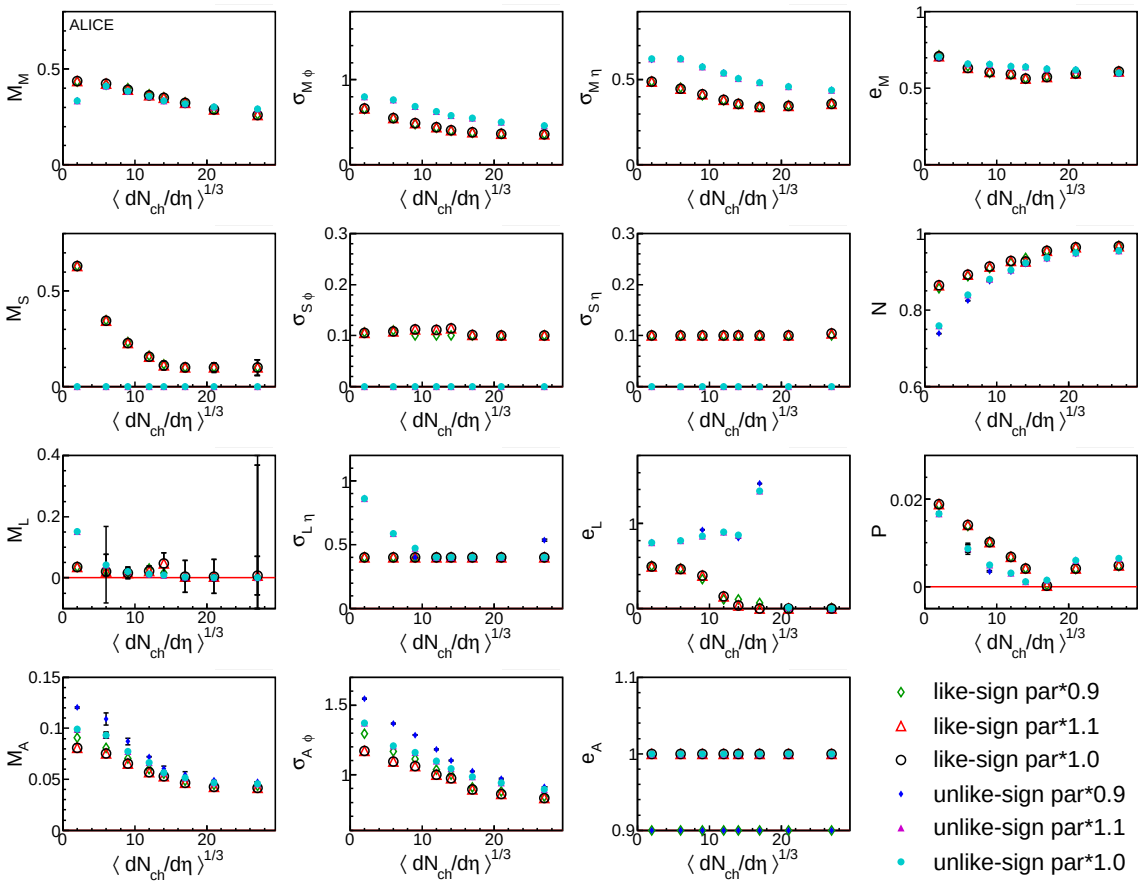

Figure 7.6: Comparison of fit parameters for 10% change of starting parameters.

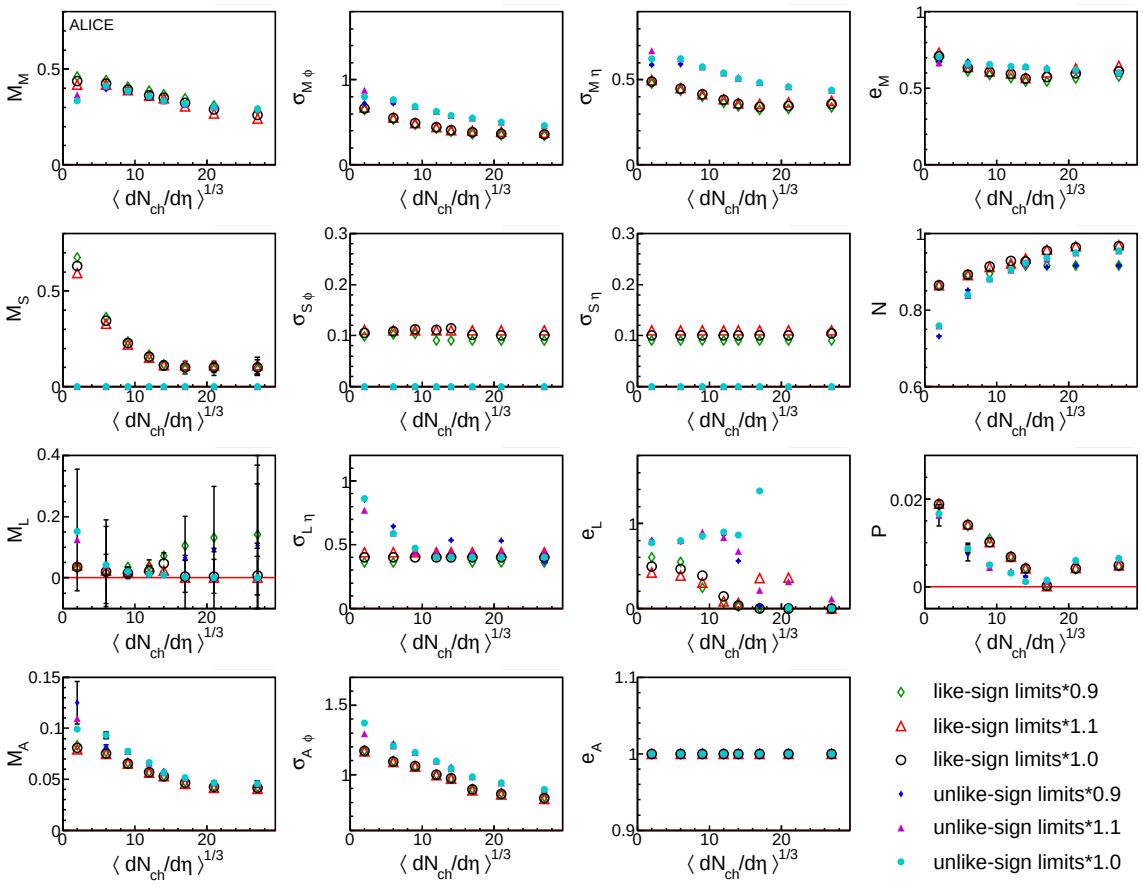

Figure 7.7: Comparison of fit parameters for 10% change of parameters limits.

Chapter 8

Conclusions

This thesis is a part of research done during my stay at CERN in summer 2011. It involves the results of fitting the $\Delta\eta\Delta\phi$ correlation function in the proton-proton collisions at center of mass energy $\sqrt{s} = 7$ TeV recorded by the ALICE experiment.

Developing the numerical methods of analysing and fitting the correlation functions, based on the ROOT environment was the main effort of this work. Another task was to find the proper fitting formula. Finally it turned out that formula composed of the modified Gaussian functions and the second order polynomial function is sufficient. Advanced methods of minimisation based on MIGRAD algorithm allowed to obtain the parameters of the fitting formula.

The final shape of the residual histograms proves that fitting works well for multiplicity and $p_{T,sum}$ dependence. Observations of the behaviour of fit parameters allowed to draw following conclusions:

- the hypothesis of the existence of the minijets correlations was confirmed,
- the difference between same-sign and unlike-sign correlation function confirms the existence of the femtoscopic effects,
- all the structures in the $\Delta\eta\Delta\phi$ correlation function are decreasing with multiplicity, where the main contribution comes from the minijets correlations and the femtoscopic correlations. In case of the minijets, for the high multiplicity events, we have many minijets produced in one collision; therefore different minijets become background for each other and the correlation per pair decreases. The fact of the decreasing femtoscopic correlation with multiplicity was studied and described in details in [10],
- the studies in the $p_{T,sum}$ dependence allowed to distinguish the correlations coming from minijets and femtoscopy. For low $p_{T,sum}$ dominant contribution to the near-side peak are given by the femtoscopic effects, which are decreasing with $p_{T,sum}$, while minijet effects are growing with $p_{T,sum}$,

- near-side peak has non-Gaussian shape. Gaussian function modified by an additional exponent reproduces this shape well,
- longitudinal ridge is observed only in case of unlike-sign pairs of particles and low multiplicity,
- tendencies of minijet-peak and away-side ridge are directly related. It indicates the same source of those structures - production of the minijets.

Bibliography

[1] http://press.web.cern.ch

[2] http://root.cern.ch/

[3] ALICE Collaboration. *Alice Technical Design Report of the Inner Tracking System (ITS).* CERN, 1999.

[4] K. Aamodt et al. [ALICE Collaboration], *The ALICE Experiment at the CERN LHC*, JINST 3 (2008) S08002.

[5] K. Grebieszkow. *Heavy Ion Physics Lecture*, http://www.if.pw.edu.pl/ kperl/.

[6] ALICE Collaboration. *Alice Technical Design Report of the Time Projection Chamber (TPC).* CERN, 2000

[7] ALICE Collaboration. *ALICE Technical Design Report on Forward Detectors: FMD, V0, T0.* Technical report, CERN, 2004

[8] R. Fletcher, Comput. J. 13(1970) 317,

[9] F. James and M. Roos, *Minuit: A System for Function Minimization and Analysis of the Parameter Errors and Correlations*, Comput. Phys. Commun. 10 no. 6, (1975) 343–367.

[10] K. Aamodt et al. [ALICE Collaboration], *Femtoscopy of pp collisions at* $\sqrt{s} = 0.9$ *and 7 TeV at the LHC with two-pion Bose-Einstein correlations*, arXiv:1101.3665v1 [hep-ex]